applied sciences

MDPI

Article

Influence of Calibration Artefact Geometry on Pixel-Based Dimensional Measurements in Optical Microscopy

Dmytro Malakhov *, Tatiana Kelemenová and Michal Kelemen

Faculty of Mechanical Engineering, Technical University of Kosice, Letna 9, 04200 Kosice, Slovakia; tatiana.kelemenova@tuke.sk (T.K.); michal.kelemen@tuke.sk (M.K.)

* Correspondence: dmytro.malakhov@tuke.sk

Abstract

Calibration is a critical step in image-based dimensional metrology because the calibration coefficient directly determines the conversion between image pixels and physical dimensions. While numerous artefact models are available for optical microscopes, the influence of calibration artefact geometry on measurement performance has not been sufficiently investigated. This study evaluates the effect of linear and circular calibration artefacts on the calibration and verification of a pixel-based optical measuring microscope. Calibration coefficients were determined using linear and circular artefacts with nominal dimensions of 1.000 mm, 0.500/0.508 mm, and 0.200 mm at four objective magnifications (1×–4×). The calibrated microscope was subsequently verified using independent Grade 1 ceramic gauge blocks with nominal dimensions of 1.00504 mm, 1.29999 mm, and 1.50007 mm. Statistical evaluation was performed using Kruskal–Wallis testing, Dunn–Šidák post hoc analysis, effect size assessment, and measurement uncertainty analysis. The results demonstrated that calibration artefact geometry influences the obtained calibration coefficients and can produce statistically significant differences in dimensional measurements. However, uncertainty analysis revealed that the dominant contribution to the uncertainty budget originated from the microscope maximum permissible error, whereas the contribution of calibration artefact geometry remained comparatively small. All verification measurements remained within the declared metrological performance of the microscope. For the investigated microscope and experimental conditions, both calibration target geometries provided satisfactory calibration performance for the investigated microscope and measurement conditions.

Keywords: optical metrology; optical microscope calibration; calibration artefact; dimensional measurement; image-based measurement; measurement uncertainty; machine vision metrology

Check for updates

Received: 22 June 2026
Revised: 21 July 2026
Accepted: 22 July 2026
Published: 24 July 2026

Copyright: © 2026 by the authors. Licensee MDPI, Basel, Switzerland. This article is an open access article distributed under the terms and conditions of the Creative Commons Attribution (CC BY) license.

1. Introduction

The continuous development of modern manufacturing technologies, microelectronics, biomedical engineering, and precision mechanics has significantly increased the demand for reliable dimensional measurements of micro-scale and small-scale components. The continuous trend toward miniaturization requires measurement systems capable of providing high spatial resolution, non-contact operation, and metrological traceability. Among various optical measurement techniques, digital optical microscopes and machine vision-based measuring systems have become widely applied due to their ability to rapidly acquire images, automatically process geometrical information, and perform dimensional evaluations without physically contacting the measured object [1–6].

Unlike conventional optical microscopes, where dimensional evaluation depends on the operator's visual interpretation, modern digital measuring microscopes employ image sensors and computational algorithms to determine geometrical features directly from acquired images. The measurement process is based on the conversion of image coordinates expressed in pixels into physical dimensions expressed in units of length. Therefore, the accuracy of the final measurement strongly depends on the determination of the calibration coefficient, which establishes the relationship between the image pixel coordinate system and the corresponding real-world dimensions [7–10].

For a one-dimensional measurement, the physical dimension of the evaluated feature can be expressed as

$$L = N_{\text{pix}} \cdot S_{\text{pix}}, \quad (1)$$

where L represents the measured dimension (μm), N_{pix} is the number of pixels corresponding to the evaluated feature, and S_{pix} is the calibration coefficient expressed in μm/pixel. The calibration coefficient is determined using a traceable calibration artefact with a known nominal dimension and depends on several factors, including the optical magnification, camera sensor characteristics, image acquisition conditions, and optical configuration of the microscope [11–14].

The influence of magnification is particularly important in pixel-based optical metrology because every change in objective lens or optical configuration modifies the field of view and the effective pixel size. In general, higher magnifications provide a smaller pixel-to-length ratio and enable more accurate localization of feature boundaries. However, higher magnifications generally improve spatial resolution and edge localization; however, the measurements may also become more sensitive to image-quality degradation caused by lens distortion, defocus resulting from inaccurate focusing, non-uniform illumination, and mechanical vibrations. These factors can influence edge localization accuracy and consequently affect the determination of calibration coefficients and dimensional measurements. Conversely, lower magnifications provide a larger measurement area and improved robustness against certain disturbances, but they reduce the number of pixels representing the measured feature and may decrease the achievable dimensional resolution [15–18].

Accurate calibration is a prerequisite for reliable dimensional measurements in digital optical microscopy. It establishes the conversion factor between image pixels and physical dimensions while simultaneously accounting for the characteristics of the optical system. Consequently, both the geometry and the dimensions of the calibration artefact may influence the resulting measurement accuracy and uncertainty [19–22].

The calibration of optical measuring systems has traditionally been performed using various reference targets, including line scales, stage micrometers, grid patterns, and circular or dot-based calibration standards. Each type of artefact provides different metrological information. Linear standards establish direct traceability for one-dimensional length measurements and are commonly used for determining the pixel scale coefficient. In contrast, circular and two-dimensional calibration patterns allow the evaluation of additional geometric properties, such as feature localization from multiple directions, spatial distribution of measurement errors, and compensation of certain optical distortions [23–27].

Recent developments in machine vision and camera calibration have demonstrated that the geometry of the calibration pattern may significantly influence the stability and robustness of feature extraction algorithms. For example, sub-pixel determination of line edges depends on image contrast, thresholding methods, and edge fitting algorithms, whereas circular features can be evaluated using mathematical models such as least-squares circle fitting, which may provide improved resistance to random image noise [28–31]. Consequently, different calibration artefacts may produce different calibration coefficients and may lead to variations in the final dimensional measurement results.

The quality of dimensional measurements performed by digital optical systems is not determined solely by the calibration coefficient itself but also by the associated measurement uncertainty and the overall metrological performance of the instrument. According to the principles of measurement uncertainty evaluation described in the Guide to the Expression of Uncertainty in Measurement (GUM), the final measurement result should include all significant uncertainty contributions arising from the measuring instrument, calibration procedure, environmental conditions, and data processing algorithms [13,32–35]. The combined standard uncertainty can be expressed as:

$$u_c = \sqrt{\sum_{i=1}^{n} (c_i u_i)^2}, \quad (2)$$

where u_i represents the individual standard uncertainty components and c_i denotes the corresponding sensitivity coefficients describing their influence on the final measured quantity. The expanded uncertainty U, representing the interval expected to contain the true value with a specified confidence level, is determined by:

$$U = k \cdot u_c, \quad (3)$$

where k is the coverage factor, typically equal to 2 for a confidence level of approximately 95%.

In digital microscopy, the uncertainty budget includes multiple contributions related to the imaging process. These components may originate from the uncertainty of the calibration artefact, repeatability of image acquisition, sub-pixel feature localization, optical distortions, illumination variations, focusing conditions, and mechanical stability of the measuring system [36–39]. Consequently, the selection of a calibration artefact cannot be considered only as a matter of traceability but also as a potential source affecting the overall uncertainty of the measurement system.

The metrological performance of optical microscopes is commonly characterized by the maximum permissible error (MPE) specified by the manufacturer or verified according to established standards for optical coordinate measuring systems [40–42]. The MPE defines the largest acceptable deviation of the measured value from the reference dimension under specified operating conditions and represents an important criterion for evaluating instrument performance. Nevertheless, compliance with the declared MPE does not necessarily guarantee that different calibration strategies will provide equivalent measurement results. Two microscopes operating within their permissible limits may still exhibit different sensitivity to calibration procedures due to variations in optical design, detector characteristics, image processing algorithms, and mechanical construction.

A considerable amount of research has been dedicated to the calibration of optical measuring systems, camera models, sub-pixel edge detection, and uncertainty evaluation in machine vision applications [43–47]. Previous studies have demonstrated that linear scales, grid patterns, circular targets, and other geometrical artefacts can provide reliable dimensional references depending on the measurement task and the calibration methodology [48–52]. Linear calibration standards are traditionally preferred for one-dimensional length calibration because they provide direct traceability to known distances. However, the measurement of line features is strongly influenced by edge localization methods, image contrast, and the determination of the exact position of the calibration marks [53,54].

On the other hand, circular calibration artefacts have gained increasing attention in machine vision and optical metrology because the determination of the circle center and diameter can be achieved using robust mathematical fitting algorithms involving information from multiple points distributed along the entire circumference [55–58]. Such an

approach can reduce the influence of local image noise and improve the repeatability of sub-pixel feature extraction. Furthermore, circular and two-dimensional calibration patterns can provide additional information regarding image distortion and spatial variations in measurement errors across the field of view [59,60].

Despite extensive developments in optical dimensional metrology, current research primarily focuses on improving calibration algorithms, enhancing sub-pixel edge detection, and reducing uncertainty contributions. However, a systematic experimental comparison of how the geometry of calibration artefacts influences the calibration coefficient, dimensional measurement error, and uncertainty of digital optical microscopes with different maximum permissible errors has not been sufficiently investigated. In particular, there is a lack of studies evaluating whether the selection between linear and circular calibration standards leads to measurable differences in the metrological performance of microscopes operating on the same pixel-based measurement principle but having different declared accuracy classes.

Therefore, the aim of this study is to investigate the influence of calibration artefact geometry on the metrological characteristics of a pixel-based digital optical microscope. Linear and circular calibration artefacts were used to determine calibration coefficients at multiple magnification levels. The influence of the selected calibration strategy was subsequently assessed through measurements of independent ceramic gauge blocks, enabling the practical impact of calibration artefact geometry on dimensional measurement accuracy, statistical significance, and measurement uncertainty to be evaluated.

Based on the identified research gap, the following research criteria are defined:

Criterion 1: Determination of the influence of calibration artefact geometry on the calibration coefficient of pixel-based optical microscopes at different magnifications.

Criterion 2: Evaluation of whether the use of linear and circular calibration standards leads to statistically significant differences in the measured dimensions and measurement errors obtained from an independent verification artefact.

Criterion 3: Analysis of the relationship between calibration artefact geometry and the expanded measurement uncertainty for microscopes with different maximum permissible errors.

This work provides the following main contributions:

- A comprehensive experimental comparison of linear and circular calibration artefacts for pixel-based optical microscopy.
- An analysis of the influence of calibration artefact geometry on calibration coefficients, dimensional errors, and measurement uncertainty at various magnification levels.
- An evaluation of the influence of calibration artefact geometry on calibration coefficients, dimensional deviations, statistical significance, and measurement uncertainty.
- Practical recommendations regarding the selection of suitable calibration artefacts for achieving reliable and traceable dimensional measurements.

The remainder of this paper is organized as follows. Section 2 describes the experimental setup, characteristics of the investigated microscopes, calibration artefacts, and measurement procedure. Section 3 presents the calculation of calibration coefficients, verification measurements, and uncertainty evaluation. Section 4 discusses the influence of calibration artefact geometry, calibration dimension, and magnification on the obtained measurement results. Finally, Section 5 summarizes the main findings and provides recommendations for practical implementation in optical dimensional metrology.

2. Materials and Methods

This study was designed to investigate the influence of calibration artefact geometry and calibration length on the performance of a pixel-based optical measuring microscope.

Two calibration artefacts with different geometrical characteristics, namely a linear artefact and a circular artefact, were used to determine calibration coefficients at four magnification levels. The nominal dimensions specified by the manufacturer were used for calibration. The calibration targets themselves were not re-calibrated within the scope of this study. The obtained calibration coefficients were subsequently applied to the measurement of independent reference standards in order to evaluate their influence on dimensional measurement accuracy. Independent verification was performed using Grade 1 ceramic gauge blocks with calibrated reference values, ensuring that the evaluation of calibration performance was independent of the calibration targets.

The experimental procedure consisted of three main stages: calibration coefficient determination, comparison of calibration coefficients obtained from different artefacts, and verification measurements using independent ceramic gauge blocks.

2.1. Optical Measuring System

The experimental investigation was performed using a digital optical measuring microscope. The microscope operates on the principle of pixel-based dimensional measurement, where dimensions are determined from digital images acquired by an integrated camera system. The measured dimensions are obtained by converting distances expressed in pixels into physical dimensions using a calibration coefficient. The microscope employs an integrated zoom imaging lens (0.6×–5×) coupled with a CMOS image sensor rather than interchangeable finite- or infinity-corrected microscope objectives. Therefore, the present study is based on a digital image-based measuring system with an integrated optical configuration.

The microscope provides four objective magnification levels. For each objective, the manufacturer specifies the corresponding image magnification and maximum permissible error (MPE). The technical characteristics of the microscope are summarized in Table 1.

Table 1. Technical characteristics of the optical measuring microscope.

Objective Magnification	Image Magnification	MPE (μm)
1×	40.9×	±6
2×	81.8×	±6
3×	122.7×	±5
4×	163.6×	±4

A photograph of the optical measuring microscope used in the experiments is shown in Figure 1.

All measurements were performed in an air-conditioned metrology laboratory under controlled environmental conditions. The laboratory temperature was maintained at (20 ± 1) °C, while the relative humidity was maintained within 40–60%. Prior to the measurements, the optical microscope, calibration targets, and Grade 1 ceramic gauge blocks were stored in the laboratory for 24 h to ensure complete thermal stabilization and to minimize the influence of thermal expansion on the measurement results. Throughout the experimental campaign, stable illumination conditions were maintained, and care was taken to minimize external vibrations and direct air flow that could affect measurement repeatability. The optical configuration, illumination settings, image acquisition parameters, and software settings remained unchanged throughout the entire experiment to ensure consistency of the obtained results.



Figure 1. Digital optical measuring microscope used in the experimental investigation.

2.2. Calibration Artefacts

Two calibration artefacts with different geometrical characteristics were used in this study: a linear calibration artefact and a circular calibration artefact. Both calibration targets have a declared maximum permissible error of ±1 µm. The linear and circular calibration targets were commercially manufactured glass calibration targets purchased from a scientific equipment supplier. These targets were selected because they represent commonly used calibration standards for image-based optical measurement systems. Their manufacturer-specified nominal dimensions were used during the calibration procedure.

The linear calibration artefact contains certified reference lengths of 1.000 mm, 0.500 mm, and 0.200 mm. The circular calibration artefact contains certified diameters of 1.000 mm, 0.508 mm, and 0.200 mm.

Photographs of both calibration artefacts are shown in Figure 2.

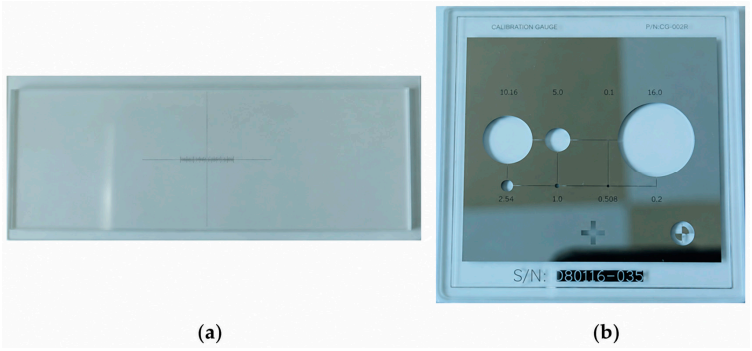


Figure 2. Calibration artefacts used in the study: (**a**) linear calibration artefact and (**b**) circular calibration artefact.

The selected dimensions were chosen to investigate the influence of calibration length on the determination of the pixel calibration coefficient. Furthermore, the use of two geometrically different artefacts allowed the evaluation of the influence of calibration artefact geometry on the calibration process.

2.3. Calibration Procedure

The calibration procedure was performed separately for each magnification level and each calibration dimension. For every calibration condition, ten repeated measurements were carried out.

The calibration coefficient was determined as

$$S_{\text{pix}} = \frac{L_{\text{ref}}}{N_{\text{pix}}}, \tag{4}$$

where S_{pix} is the calibration coefficient expressed in mm/pixel, L_{ref} is the certified reference dimension of the calibration artefact, and N_{pix} is the measured dimension expressed in pixels.

For each calibration condition, the arithmetic mean calibration coefficient was calculated according to

$$\overline{S}_{\text{pix}} = \frac{1}{n}\sum_{i=1}^{n} S_{\text{pix},i}, \tag{5}$$

where $n = 10$.

The repeatability of the calibration process was evaluated using the sample standard deviation

$$s = \sqrt{\frac{\sum_{i=1}^{n}\left(S_{\text{pix},i} - \overline{S}_{\text{pix}}\right)^2}{n-1}}, \tag{6}$$

The obtained mean calibration coefficients and corresponding standard deviations are summarized in Table 2.

Table 2. Mean calibration coefficients and standard deviations obtained for the investigated calibration artefacts.

Artefact Type	Nominal Dimension (mm)	Statistic	1×	2×	3×	4×
Linear	1.000	Mean (mm/pix)	0.00609933	0.00301631	0.00200930	0.00149252
		SD (mm/pix)	0.000035	0.000017	0.000029	0.000009
Linear	0.500	Mean (mm/pix)	0.00605917	0.00303430	0.00202755	0.00150099
		SD (mm/pix)	0.000116	0.000051	0.000019	0.000010
Linear	0.200	Mean (mm/pix)	0.00620572	0.00305420	0.00181292	0.00151359
		SD (mm/pix)	0.000229	0.000102	0.000569	0.000033
Circular	1.000	Mean (mm/pix)	0.00587360	0.00303128	0.00199667	0.00149259
		SD (mm/pix)	0.000011	0.000027	0.000003	0.000012
Circular	0.508	Mean (mm/pix)	0.00593119	0.00299189	0.00198753	0.00148985
		SD (mm/pix)	0.000017	0.000004	0.000003	0.000002
Circular	0.200	Mean (mm/pix)	0.00575888	0.00294312	0.00195283	0.00147243
		SD (mm/pix)	0.000035	0.000010	0.000002	0.000009

The calibration coefficients presented in Table 2 were subsequently used to convert pixel measurements into physical dimensions during the verification stage.

To evaluate the influence of calibration artefact geometry, the difference between calibration coefficients obtained using the linear and circular calibration artefacts was additionally calculated as

$$\Delta S_{\text{pix}} = S_{\text{pix,Linear}} - S_{\text{pix,Circular}}, \tag{7}$$

where $S_{\text{pix,Linear}}$ and $S_{\text{pix,Circular}}$ represent the calibration coefficients obtained from the linear and circular calibration artefacts, respectively.

The calculated differences are summarized in Table 3.

Table 3. Difference between calibration coefficients obtained using linear and circular calibration artefacts (µm/pixel).

Nominal Dimension (mm)	1×	2×	3×	4×
1.000	0.22573	−0.01498	0.01263	−0.00007
0.508 *	0.12798	0.04241	0.04001	0.01113
0.200	0.44684	0.11108	−0.13991	0.04116

* For the circular calibration artefact, the nominal diameter was 0.508 mm, while the corresponding linear calibration length was 0.500 mm. Note: Positive values indicate that the calibration coefficient obtained using the linear target is larger than that obtained using the circular target, whereas negative values indicate the opposite.

All image acquisition, edge localization, pixel counting, and dimensional measurements were performed using the proprietary software supplied with the microscope. The software automatically identifies the measurement edges after the operator selects the calibration feature and determines the corresponding pixel distance. Since the image-processing algorithms are implemented internally by the manufacturer, detailed information regarding the edge-detection procedure is not available to the user. No external image-processing software or custom image-analysis algorithms were employed.

Dimensional measurements were performed using the proprietary software supplied with the optical measuring microscope. During each calibration and verification measurement, the operator manually selected the corresponding geometric features (line endpoints or circular feature) directly on the acquired microscope image. The software subsequently calculated the corresponding distance or diameter based on its internal image-processing algorithms. Since these algorithms are proprietary and are not disclosed by the manufacturer, detailed information regarding the implemented edge detection, sub-pixel interpolation, and circle-fitting procedures is not available. To ensure consistency throughout the study, all measurements were performed by the same operator using identical software settings, identical measurement procedures, and the same measurement protocol for all calibration targets and verification measurements. Therefore, any differences observed between the investigated calibration conditions originate from the calibration procedure itself rather than from changes in the image-processing algorithm or measurement settings.

2.4. Verification Measurements Using Independent Reference Standards

The verification measurements were performed using three ceramic gauge blocks conforming to ISO 3650, accuracy grade 1 [61]. According to the calibration certificate, the gauge blocks possess a maximum permissible error of ±0.20 µm. The nominal dimensions of the gauge blocks were 1.005 mm, 1.300 mm, and 1.500 mm.

To ensure traceability of the verification measurements, the conventional true values of the gauge blocks were determined from the nominal dimensions and the corresponding systematic errors reported in the calibration certificate according to

$$L_{\text{true}} = L_{\text{nom}} - e_{\text{sys}}, \tag{8}$$

where L_{true} is the conventional true value of the gauge block, L_{nom} is the nominal dimension, and e_{sys} is the systematic error reported in the calibration certificate.

The resulting conventional true values used throughout the verification procedure are summarized in Table 4.

Table 4. Reference values of the ceramic gauge blocks used for verification measurements.

Nominal Value (mm)	Systematic Error (µm)	Conventional True Value (mm)
1.005	−0.04	1.00504
1.300	+0.01	1.29999
1.500	−0.07	1.50007

A photograph of the ceramic gauge blocks used in the study is shown in Figure 3.



Figure 3. Ceramic gauge blocks used as independent verification standards.

The gauge blocks were not used during calibration and therefore provided an independent assessment of the calibration coefficients obtained from the investigated calibration artefacts.

For each magnification level, the microscope was calibrated using each calibration artefact and calibration dimension. Subsequently, each gauge block was measured ten times.

The measured dimension was calculated as

$$L_{\text{meas}} = N_{\text{pix}} \cdot \overline{S}_{\text{pix}}, \tag{9}$$

where L_{meas} is the measured dimension of the gauge block, N_{pix} is the measured pixel dimension, and $\overline{S}_{\text{pix}}$ is the corresponding calibration coefficient.

The deviation from the nominal value was determined as

$$E = L_{\text{meas}} - L_{\text{true}}, \tag{10}$$

where E is the measurement deviation

The obtained deviations were used as the primary indicator for evaluating the influence of calibration artefact geometry and calibration length on measurement performance.

2.5. Data Processing and Statistical Analysis

The statistical analysis was performed to evaluate the influence of calibration artefact geometry, calibration length, and magnification level on the dimensional measurement performance of the optical microscope.

For each calibration and verification dataset, ten repeated measurements were performed. The arithmetic mean was calculated as

$$\overline{x} = \frac{1}{n} \sum_{i=1}^{n} x_i, \tag{11}$$

where n denotes the number of repeated measurements.

The measurement repeatability was evaluated using the sample standard deviation

$$s = \sqrt{\frac{\sum_{i=1}^{n}(x_i - \bar{x})^2}{n-1}}, \tag{12}$$

which was used as an indicator of the dispersion of repeated measurements.

For the verification measurements, the measurement deviation was determined as (10). To enable comparison between gauge blocks of different nominal dimensions, the relative measurement deviation was additionally calculated according to

$$E_{\text{rel}} = \frac{L_{\text{meas}} - L_{\text{true}}}{L_{\text{true}}} \cdot 100\%, \tag{13}$$

where E_{rel} is expressed as a percentage.

The standard uncertainty associated with repeatability was evaluated as

$$u_{\text{A}} = \frac{s}{\sqrt{n}}, \tag{14}$$

where s is the sample standard deviation and n is the number of repeated measurements.

The combined standard uncertainty was determined by combining the Type A and Type B uncertainty contributions according to

$$u_c = \sqrt{u_{\text{A}}^2 + u_{\text{B}}^2}, \tag{15}$$

where u_{B} includes uncertainty contributions associated with the calibration artefacts and the reference gauge blocks.

The expanded uncertainty was subsequently calculated as

$$U = k \cdot u_{\text{c}}, \tag{16}$$

where the coverage factor $k = 2$ corresponds to an approximate confidence level of 95%.

Due to the limited number of repeated measurements (n = 10) and the discrete nature of pixel-based measurements, non-parametric statistical methods were selected for hypothesis testing. Statistical significance was evaluated using the Kruskal–Wallis test followed by Dunn–Šidák multiple comparison analysis.

To investigate the influence of calibration artefact geometry and calibration length on the measurement results, the Kruskal–Wallis test was employed. This non-parametric statistical test was selected because it does not require normally distributed data and enables comparison of multiple independent groups.

The null hypothesis was defined as follows:

H0. *The calibration artefact geometry and calibration length do not produce statistically significant differences in the measurement results.*

The alternative hypothesis was defined as:

H1. *At least one calibration condition produces statistically different measurement results.*

The significance level was set to α = 0.05. Differences were considered statistically significant when the corresponding p-value was less than 0.05.

When statistically significant differences were identified by the Kruskal–Wallis test, post hoc multiple comparison analysis was performed to determine which calibration conditions differed significantly from each other.

All statistical analyses were performed using MATLAB R2026a (MathWorks, Natick, MA, USA).

The overall experimental methodology adopted in this work is summarized in Figure 4. The workflow illustrates the sequence of calibration, verification, statistical evaluation, and uncertainty analysis applied throughout the investigation.

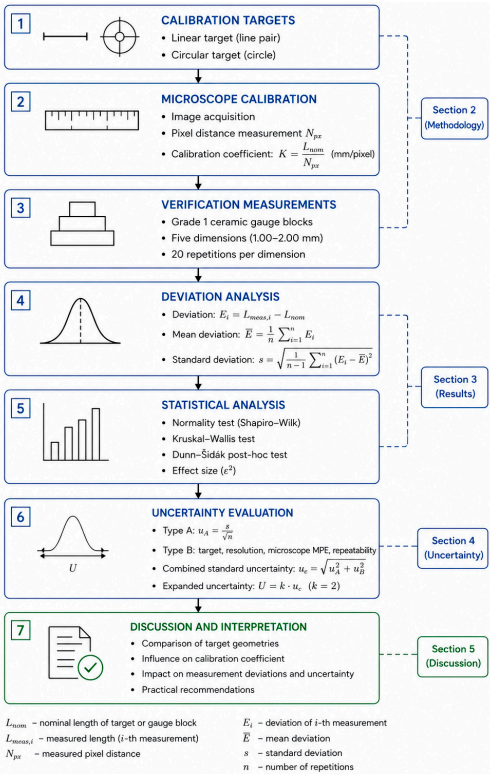


Figure 4. Experimental workflow of the proposed methodology.

3. Evaluation of Calibration Artefact Geometry

This section presents the experimental evaluation of the influence of calibration artefact geometry and calibration length on the dimensional measurement performance of the optical microscope. The analysis is divided into several stages. First, the calibration coefficients obtained from the linear and circular calibration artefacts are compared to different magnification levels. Subsequently, the differences between the calibration coefficients are evaluated to identify the effect of artefact geometry on the calibration process. The obtained calibration coefficients are then applied to the measurement of independent ceramic gauge blocks to assess their influence on measurement accuracy. Finally, statistical analyses and uncertainty evaluations are performed to determine whether the observed differences are statistically significant and metrologically relevant.

3.1. Calibration Coefficients Obtained from Linear and Circular Artefacts

The first stage of the experimental investigation focused on the determination of calibration coefficients obtained using linear and circular calibration artefacts. For each calibration artefact dimension and magnification level, ten repeated measurements were performed. The resulting arithmetic means and standard deviations are summarized in Table 2.

To facilitate comparison, Figure 5 illustrates the mean calibration coefficients obtained for all investigated calibration conditions.

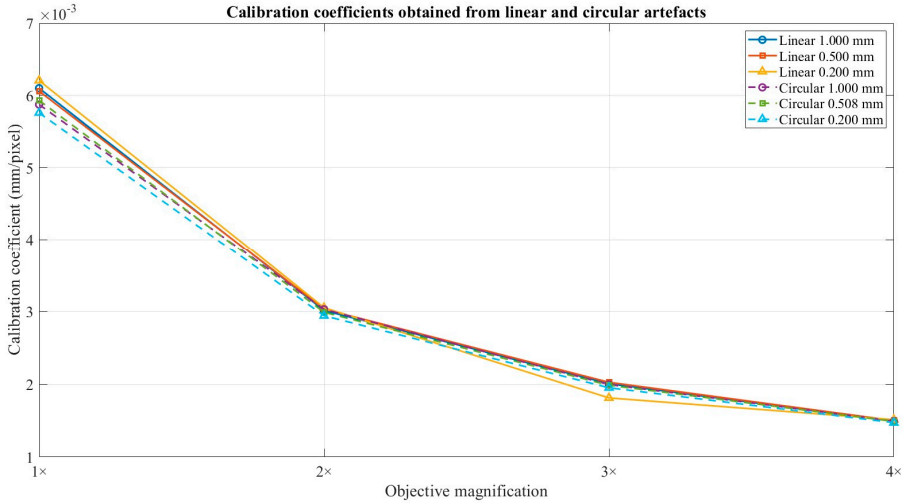


Figure 5. Calibration coefficients obtained using linear and circular calibration artefacts at different objective magnifications.

The calibration coefficients obtained for all investigated calibration artefacts are presented in Figure 5. As expected, the calibration coefficient decreased with increasing magnification for all calibration conditions. This behaviour is consistent with the operating principle of image-based dimensional measurements, where a higher optical magnification reduces the physical dimension represented by a single image pixel.

For the 1.000 mm calibration dimension, both linear and circular calibration artefacts produced similar calibration coefficients across all magnification levels. At 1× magnification, the calibration coefficients were 0.006099 mm/pixel and 0.005874 mm/pixel for the linear and circular artefacts, respectively. The difference between the two artefacts decreased substantially at higher magnifications.

A similar trend was observed for the intermediate calibration dimensions of 0.500 mm and 0.508 mm. The calibration coefficients remained close to each other over the entire magnification range, indicating comparable calibration performance for both artefact geometries.

The largest deviations were observed for the smallest calibration dimension of 0.200 mm. In particular, the linear artefact produced a calibration coefficient of 0.001813 mm/pixel at 3× magnification, whereas the corresponding circular artefact yielded 0.001953 mm/pixel. This difference suggests that measurements based on small calibration features may be more sensitive to feature localization and image-processing effects.

Overall, the results indicate that the influence of calibration artefact geometry on the calibration coefficient is relatively small compared to the influence of magnification. Nevertheless, measurable differences between calibration conditions were observed and are further analysed in the following sections.

3.2. Comparison of Calibration Coefficients

To evaluate the influence of calibration artefact geometry on the calibration process, the differences between the calibration coefficients obtained using the linear and circular calibration artefacts were calculated according to Equation (4). The resulting differences are summarized in Table 3 and graphically presented in Figure 6.

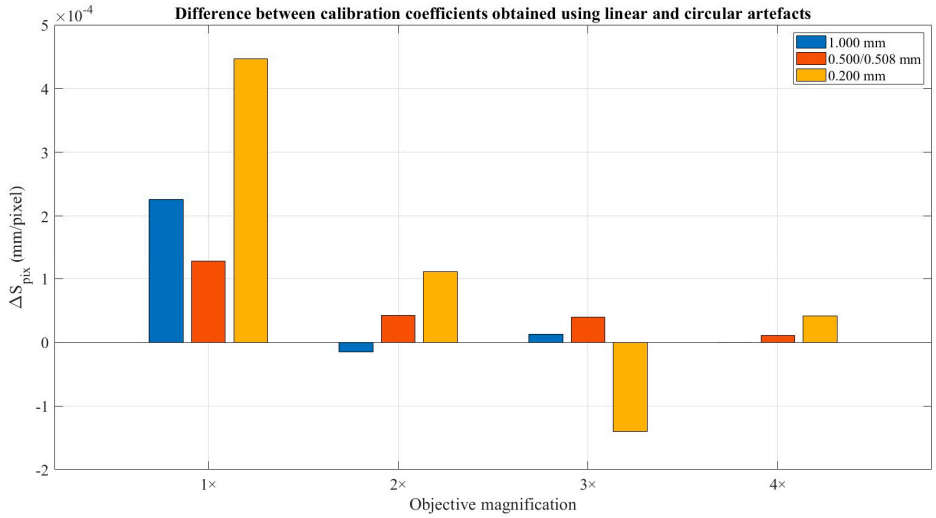


Figure 6. Difference between calibration coefficients obtained using linear and circular calibration artefacts at different magnification levels.

Figure 6 illustrates the variation in the calibration coefficient difference, ΔS_{pix}, as a function of magnification and calibration dimension. Positive values indicate that the calibration coefficient obtained from the linear artefact is greater than the corresponding coefficient obtained from the circular artefact, whereas negative values indicate the opposite behaviour.

The largest differences were observed at the lowest magnification level (1×) for all investigated calibration dimensions. In particular, the 0.200 mm calibration dimension exhibited the greatest discrepancy between artefact geometries, reaching a difference of 0.000447 mm/pixel. Similarly, the 1.000 mm calibration dimension produced a difference of 0.000226 mm/pixel, while the intermediate calibration dimension of approximately 0.5 mm yielded a smaller difference of 0.000128 mm/pixel.

As the magnification increased, the differences between the calibration coefficients generally decreased. At 2× magnification, all calibration dimensions exhibited substantially lower ΔS_{pix} values compared to those obtained at 1× magnification. This behaviour suggests that the influence of calibration artefact geometry becomes less pronounced as the effective image resolution increases.

At 3× magnification, distinct behaviour was observed for the smallest calibration dimension. While the 1.000 mm and 0.500/0.508 mm dimensions remained associated with positive differences, the 0.200 mm dimension exhibited a negative value of −0.000140 mm/pixel. This result indicates that the circular calibration artefact produced a larger calibration coefficient than the corresponding linear artefact under these conditions. Such behaviour may be attributed to the increased sensitivity of small calibration features to edge localization, image noise, and sub-pixel feature extraction.

At the highest magnification level (4×), the differences between calibration coefficients became very small for all investigated dimensions. The difference for the 1.000 mm calibration dimension was practically zero, while the remaining dimensions exhibited values below 0.00005 mm/pixel. These results indicate that the influence of calibration artefact geometry is considerably reduced at higher magnifications.

A comparison of the three calibration dimensions further demonstrates that the smallest calibration feature (0.200 mm) consistently exhibited the largest variability between artefact geometries. In contrast, the intermediate calibration dimensions (0.500 mm and 0.508 mm) produced the most stable behaviour across all magnification levels. This observation suggests that calibration based on very small geometrical features may be more

susceptible to image-processing effects and feature localization uncertainties than calibration performed using larger reference dimensions.

Overall, the results presented in Figure 6 indicate that both calibration artefact geometry and calibration dimension influence the determination of the calibration coefficient. However, the magnitude of this influence decreases with increasing magnification and becomes negligible at 4× magnification. Since the calibration coefficient directly affects all subsequent dimensional measurements, the practical significance of these differences must be evaluated through measurements of independent reference standards.

Therefore, the calibration coefficients obtained from both calibration artefacts were subsequently applied to the measurement of certified ceramic gauge blocks to determine whether the observed differences propagate into measurable deviations in dimensional measurements.

3.3. Verification Measurements Using Independent Gauge Blocks

The calibration coefficients obtained from the linear and circular calibration artefacts were subsequently applied to the measurement of independent ceramic gauge blocks. The purpose of this verification procedure was to determine whether the differences observed during calibration propagate into dimensional measurements performed on independent reference standards.

The verification measurements were carried out using three ceramic gauge blocks with conventional true values of 1.00504 mm, 1.29999 mm, and 1.50007 mm. For each magnification level and calibration condition, ten repeated measurements were performed. The resulting measurement deviations are summarized in Table 5 and graphically presented in Figure 7.

Table 5. Measurement deviations obtained for independent ceramic gauge blocks, $E = L_{meas} - L_{true}$, in μm.

Magnification	Calibration Condition	1.00504 mm	1.29999 mm	1.50007 mm
1×	Linear 1.000 mm	−4.81	1.22	2.63
1×	Linear 0.500 mm	−1.47	−0.87	−2.29
1×	Linear 0.200 mm	−2.54	−0.55	−2.03
1×	Circular 1.000 mm	−3.11	0.75	0.54
1×	Circular 0.508 mm	−4.57	−0.33	0.24
1×	Circular 0.200 mm	−3.90	2.11	0.63
2×	Linear 1.000 mm	−3.84	−0.92	0.49
2×	Linear 0.500 mm	−3.28	3.13	0.71
2×	Linear 0.200 mm	−3.24	−0.89	−1.57
2×	Circular 1.000 mm	−3.79	2.63	−1.27
2×	Circular 0.508 mm	−2.71	1.31	1.43
2×	Circular 0.200 mm	−1.70	1.18	−0.57
3×	Linear 1.000 mm	−1.84	1.53	0.07
3×	Linear 0.500 mm	−3.91	1.93	0.13
3×	Linear 0.200 mm	−4.34	−0.89	1.03
3×	Circular 1.000 mm	−4.14	−0.69	−0.17
3×	Circular 0.508 mm	−4.88	0.46	−0.47
3×	Circular 0.200 mm	−2.48	−1.26	1.43
4×	Linear 1.000 mm	−2.34	−0.09	−0.51
4×	Linear 0.500 mm	−2.64	1.44	2.23
4×	Linear 0.200 mm	−3.50	0.01	0.38
4×	Circular 1.000 mm	−2.58	−0.84	2.83
4×	Circular 0.508 mm	−3.46	1.71	−1.47
4×	Circular 0.200 mm	−3.74	2.03	1.49

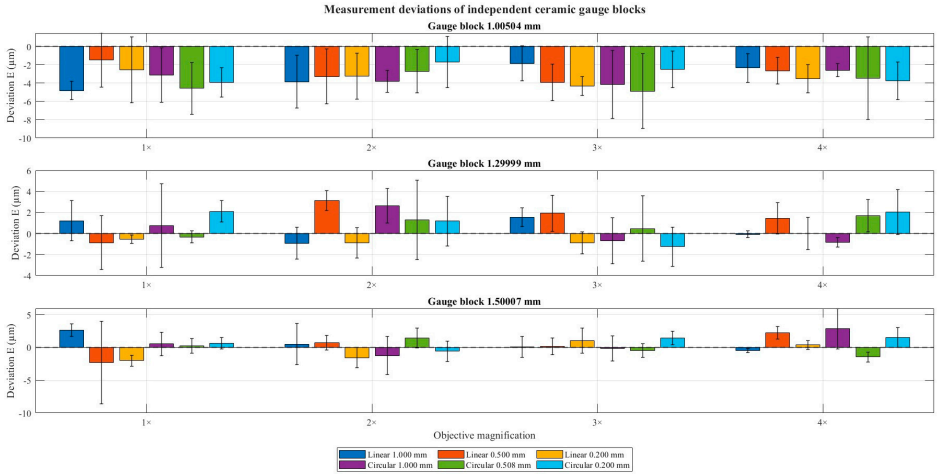


Figure 7. Measurement deviations of independent ceramic gauge blocks obtained after calibration using linear and circular calibration artefacts. Error bars represent the standard deviation of ten repeated measurements.

Figure 7 shows the measurement deviations obtained for all investigated calibration conditions. The error bars represent the standard deviation of ten repeated measurements and provide information about the repeatability of the measurement process.

For the 1.00504 mm gauge block, all measurement deviations were negative regardless of magnification or calibration condition. The measured values therefore remained systematically below the conventional true value of the gauge block. The deviations ranged approximately from −1.47 µm to −4.88 µm. The largest negative deviations were generally observed for calibration conditions involving the smallest calibration dimensions, particularly at 3× magnification. Despite the variation between calibration conditions, the overall behaviour remained relatively consistent, with all results located within a narrow deviation range of approximately 3.5 µm.

A different behaviour was observed for the 1.29999 mm gauge block. In this case, both positive and negative deviations were obtained depending on the calibration condition and magnification level. The measured deviations varied between approximately −1.26 µm and +3.13 µm. Several calibration conditions produced deviations close to zero, particularly at 4× magnification, indicating good agreement between the measured and reference values. Compared with the smallest gauge block, the influence of calibration condition appears more pronounced for this intermediate dimension.

For the largest gauge block, having a conventional true value of 1.50007 mm, the measurement deviations were generally distributed around zero. The majority of deviations remained within approximately ±3 µm. Positive and negative deviations were observed for both linear and circular calibration artefacts, suggesting that no obvious systematic bias associated with a particular calibration geometry can be identified solely from the verification measurements. The largest positive deviation was observed for the circular 1.000 mm calibration condition at 4× magnification, whereas the largest negative deviation occurred for the linear 0.500 mm calibration condition at 1× magnification.

The repeatability of the measurements can be evaluated from the error bars presented in Figure 6. In general, the standard deviations remained relatively small compared with the corresponding measurement deviations, indicating stable measurement performance under most experimental conditions. Nevertheless, several calibration conditions exhibited increased variability, particularly for measurements performed at lower magnifications. Such behaviour is expected because lower magnification levels provide a larger physical dimension per pixel and therefore increase sensitivity to edge localization and image-processing uncertainties.

A comparison of the three gauge blocks reveals that the smallest gauge block consistently produced negative measurement deviations, whereas the larger gauge blocks exhibited both positive and negative deviations. This observation suggests that the dimensional relationship between the calibration artefacts and the measured object may influence the resulting measurement error. However, the experimental results alone do not allow definitive conclusions regarding the statistical significance of these differences.

Although the observed deviations are generally within several micrometres, the magnitude and direction of the deviations vary between calibration conditions. Consequently, a statistical evaluation is required to determine whether these differences represent random variation or systematic effects associated with calibration artefact selection.

3.4. Statistical Evaluation of Calibration Artefact Geometry

To determine whether the observed differences between calibration conditions were statistically significant, a non-parametric statistical analysis was performed. Because only ten repeated measurements were available for each experimental condition and the measurement data originated from pixel-based image evaluation, no assumption of normality was imposed. Consequently, the Kruskal–Wallis test was selected as the primary statistical method for comparing measurement results obtained under different calibration conditions. The significance level was set to $\alpha = 0.05$.

The statistical evaluation consisted of Kruskal–Wallis hypothesis testing, Dunn–Šidák post hoc comparisons, and effect size analysis using the epsilon-squared coefficient.

3.4.1. Kruskal–Wallis Analysis

The Kruskal–Wallis results are summarized in Table 6 and visualized in Figure 8.

Table 6. Kruskal–Wallis test results and effect sizes.

Gauge Block	Magnification	H Statistic	*p*-Value	ε^2	Significant
1.00504 mm	1×	14.175	0.0145	0.170	Yes
1.00504 mm	2×	4.331	0.5027	0.000	No
1.00504 mm	3×	12.359	0.0302	0.136	Yes
1.00504 mm	4×	3.898	0.5642	0.000	No
1.29999 mm	1×	24.818	1.51×10^{-4}	0.367	Yes
1.29999 mm	2×	25.756	9.94×10^{-5}	0.384	Yes
1.29999 mm	3×	19.005	0.0022	0.254	Yes
1.29999 mm	4×	27.723	4.13×10^{-5}	0.421	Yes
1.50007 mm	1×	22.008	5.15×10^{-4}	0.315	Yes
1.50007 mm	2×	7.137	0.2388	0.033	No
1.50007 mm	3×	14.611	0.0122	0.178	Yes
1.50007 mm	4×	44.214	2.12×10^{-8}	0.726	Yes

The statistical analysis revealed that the influence of calibration conditions depended strongly on both the gauge block dimension and the selected magnification.

For the smallest gauge block (1.00504 mm), statistically significant differences were detected only at 1× and 3× magnification. No significant differences were observed at 2× and 4× magnification. The corresponding effect sizes were classified as moderate ($\varepsilon^2 = 0.170$ and $\varepsilon^2 = 0.136$), indicating that calibration conditions had a measurable but limited influence on the measurement results.

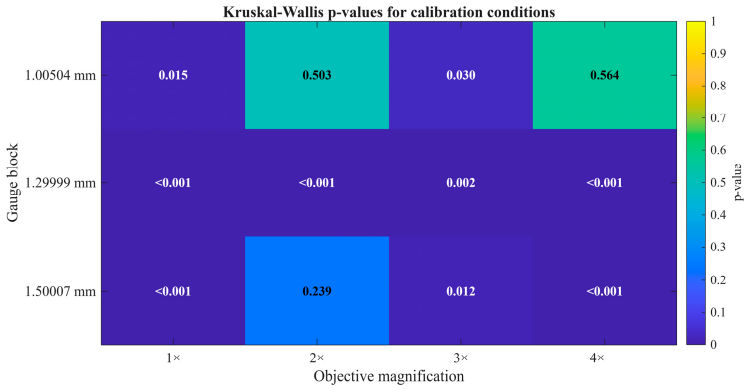


Figure 8. Kruskal–Wallis *p*-values for the comparison of calibration conditions. Values below 0.001 are displayed as <0.001.

A markedly different behaviour was observed for the intermediate gauge block (1.29999 mm). Statistically significant differences were identified at all investigated magnification levels. The calculated effect sizes ranged from $\varepsilon^2 = 0.254$ to $\varepsilon^2 = 0.421$, indicating medium-to-large effects. This gauge block therefore exhibited the highest sensitivity to calibration strategy and artefact selection.

For the largest gauge block (1.50007 mm), significant differences were observed at 1×, 3×, and 4× magnification. The strongest statistical effect of the entire study was detected at 4× magnification, where ε^2 reached 0.726 and the *p*-value decreased to 2.12×10^{-8}. In contrast, no statistically significant differences were found at 2× magnification.

Overall, nine of the twelve investigated conditions exhibited statistically significant differences between calibration strategies. The significance map shown in Figure 9 summarizes these results.

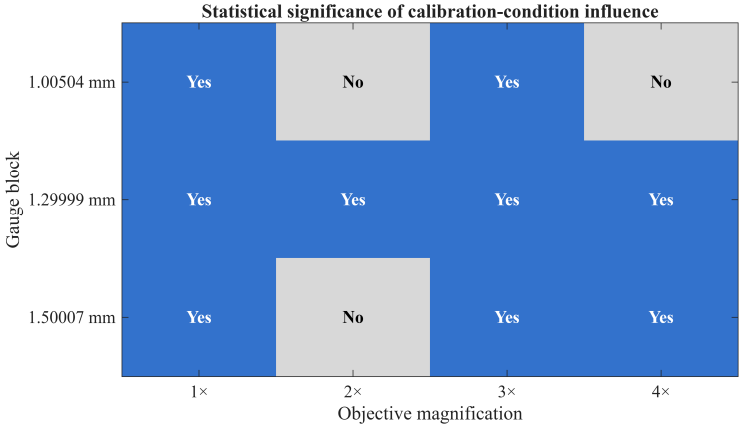


Figure 9. Statistical significance map of calibration–condition influence. Check marks indicate statistically significant differences at $\alpha = 0.05$.

Figure 9 demonstrates that the influence of calibration conditions was consistently observed for the 1.29999 mm gauge block, whereas the 1.00504 mm and 1.50007 mm gauge blocks exhibited significant effects only at selected magnifications.

3.4.2. Post Hoc Multiple Comparison Analysis

To identify which calibration conditions were responsible for the observed differences, a Dunn–Šidák post hoc multiple comparison analysis was performed for all statistically significant Kruskal–Wallis results.

The most important statistically significant pairwise comparisons are summarized in Table 7.

Table 7. Selected statistically significant pairwise comparisons obtained from the Dunn–Šidák procedure.

Gauge Block	Magnification	Comparison	Adjusted *p*-Value
1.00504 mm	1×	Circular 1.000 mm vs. Circular 0.508 mm	0.0155
1.29999 mm	1×	Linear 0.500 mm vs. Circular 0.200 mm	0.0012
1.29999 mm	1×	Linear 0.200 mm vs. Circular 0.200 mm	0.0020
1.29999 mm	2×	Linear 1.000 mm vs. Linear 0.500 mm	0.0073
1.29999 mm	2×	Linear 0.500 mm vs. Circular 0.508 mm	0.0065
1.29999 mm	3×	Linear 0.500 mm vs. Circular 0.200 mm	0.0148
1.29999 mm	4×	Circular 1.000 mm vs. Circular 0.200 mm	0.0003
1.50007 mm	1×	Linear 1.000 mm vs. Linear 0.200 mm	0.0001
1.50007 mm	3×	Linear 0.500 mm vs. Circular 0.200 mm	0.0285

The post hoc analysis revealed that the observed differences were not exclusively associated with the distinction between linear and circular artefacts. In many cases, statistically significant differences occurred between calibration conditions having different nominal dimensions, even when the artefact geometry remained identical. This observation indicates that the calibration dimension itself contributes substantially to the final measurement performance.

Particularly noteworthy is the behaviour of the 1.29999 mm gauge block, which exhibited statistically significant pairwise differences at every investigated magnification level. In contrast, the smallest gauge block produced only a single significant pairwise comparison despite exhibiting significant Kruskal–Wallis results at two magnifications.

3.4.3. Effect Size Analysis

While *p*-values indicate whether statistically significant differences exist, they do not quantify the practical magnitude of the effect. Therefore, the epsilon-squared coefficient (ε^2) was calculated for all Kruskal–Wallis tests. The resulting effect sizes are presented in Figure 10.

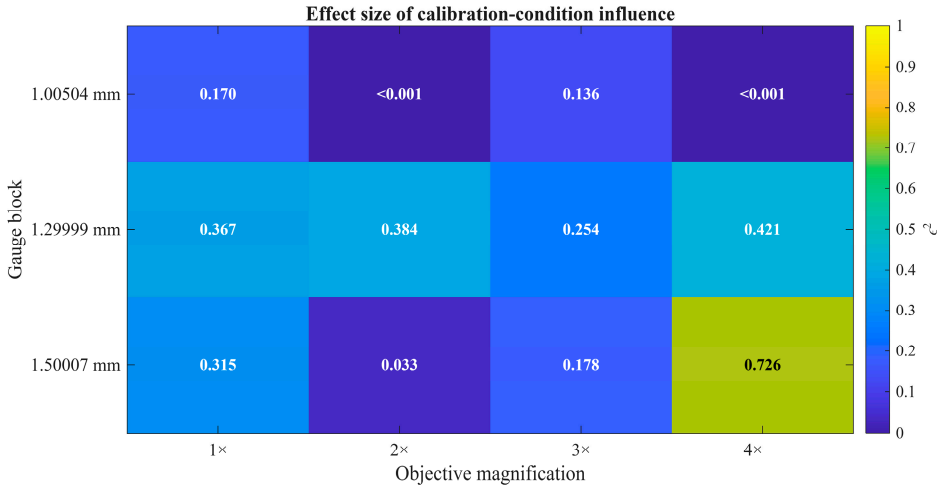


Figure 10. Effect size of calibration-condition influence expressed by epsilon-squared.

According to commonly accepted interpretation criteria ($\varepsilon^2 < 0.01$ negligible, $0.01 \leq \varepsilon^2 < 0.08$ small, $0.08 \leq \varepsilon^2 < 0.26$ medium, $\varepsilon^2 \geq 0.26$ large), the influence of calibration conditions ranged from negligible to large.

The largest effect was observed for the 1.50007 mm gauge block at 4× magnification ($\varepsilon^2 = 0.726$), indicating a very strong dependence of the measurement result on the selected calibration condition. Large effects were also obtained for the 1.29999 mm gauge block at 1×, 2×, and 4× magnification, where ε^2 exceeded 0.35.

Conversely, the 2× and 4× measurements of the 1.00504 mm gauge block produced negligible effect sizes ($\varepsilon^2 = 0.000$), confirming the absence of statistically significant differences for these experimental conditions.

The effect size analysis therefore supports the conclusions obtained from the Kruskal–Wallis test and demonstrates that the practical influence of calibration conditions is highly dependent on both magnification and measured dimension.

3.5. Measurement Uncertainty Analysis

In addition to the statistical evaluation of calibration conditions, a comprehensive uncertainty analysis was performed to quantify the metrological impact of calibration artefact geometry on dimensional measurements. The uncertainty budget was evaluated according to the principles of the Guide to the Expression of Uncertainty in Measurement (GUM) [13].

The standard uncertainty of Type A was determined from repeated measurements of the ceramic gauge blocks:

$$u_{\mathrm{A}} = \frac{s}{\sqrt{n}}, \tag{17}$$

where s is the experimental standard deviation and $n = 10$ is the number of repeated measurements.

The Type B uncertainty consisted of three independent contributions:

uncertainty associated with the calibration artefact;
uncertainty associated with the reference ceramic gauge block;
uncertainty associated with the microscope maximum permissible error (MPE).

The standard uncertainty of the calibration artefacts was determined from their specified MPE of ±1 µm assuming a rectangular distribution:

$$u_{\mathrm{cal}} = \frac{1}{\sqrt{3}} = 0.577\ \mu\mathrm{m}. \tag{18}$$

Similarly, the uncertainty contribution of the Grade 1 ceramic gauge blocks (ISO 3650) with an MPE of ±0.20 µm was calculated as

$$u_{\mathrm{GB}} = \frac{0.20}{\sqrt{3}} = 0.155\ \mu\mathrm{m}. \tag{19}$$

The uncertainty contribution associated with the microscope MPE was evaluated using the manufacturer specifications given in Table 1:

$$u_{\mathrm{MPE}} = \frac{\mathrm{MPE}}{\sqrt{3}}, \tag{20}$$

resulting in

$$\begin{aligned} u_{\mathrm{MPE},1\times} = u_{\mathrm{MPE},2\times} &= 3.464\ \mu\mathrm{m}, \\ u_{\mathrm{MPE},3\times} &= 2.887\ \mu\mathrm{m}, \\ u_{\mathrm{MPE},4\times} &= 2.309\ \mu\mathrm{m}. \end{aligned} \tag{21}$$

The manufacturer-specified maximum permissible error (MPE) was interpreted as a limiting value rather than as a statistical standard deviation. Since no experimental information regarding the probability distribution of the instrument error was available, the MPE was treated in accordance with the GUM recommendations as a limiting interval with a rectangular probability distribution. Consequently, the corresponding standard uncertainty was obtained by dividing the MPE by $\sqrt{3}$. This approach assumes that any

error within the specified tolerance interval is equally probable and is commonly applied when only the manufacturer's specification limits are available [13].

The calibration artefacts and ceramic gauge blocks are specified by maximum permissible errors rather than by experimentally determined standard deviations. In accordance with GUM recommendations, such bounded systematic effects are commonly modelled using a rectangular probability distribution [13]. For a rectangular distribution with limits ±a, the corresponding standard uncertainty is obtained as

$$u = \frac{a}{\sqrt{3}} \tag{22}$$

where a represents the half-width of the interval.

The combined Type B uncertainty was then calculated as

$$u_{\mathrm{B}} = \sqrt{u_{\mathrm{cal}}^2 + u_{\mathrm{GB}}^2 + u_{\mathrm{MPE}}^2} \tag{23}$$

and the combined standard uncertainty as

$$u_{\mathrm{c}} = \sqrt{u_{\mathrm{A}}^2 + u_{\mathrm{B}}^2}. \tag{24}$$

The expanded uncertainty was determined using a coverage factor $k = 2$:

$$U = 2u_{\mathrm{c}}. \tag{25}$$

According to ISO/IEC Guide 98-3 (GUM), the expanded uncertainty is obtained by multiplying the combined standard uncertainty by an appropriate coverage factor [13]. In the present study, a coverage factor of $k = 2$ was adopted, corresponding approximately to a coverage probability of 95%.

The uncertainty budget was evaluated for all calibration conditions and magnifications. To evaluate the relative importance of individual uncertainty sources, the uncertainty budget was calculated for each magnification level. The resulting average uncertainty components are summarized in Table 8.

Table 8. Mean uncertainty contributions for individual magnifications (all uncertainty components are expressed in µm).

Magnification	u_{A}	u_{cal}	u_{GB}	u_{MPE}	u_{B}	Mean U
1×	0.655	0.577	0.115	3.464	3.514	7.204
2×	0.674	0.577	0.115	3.464	3.514	7.173
3×	0.604	0.577	0.115	2.887	2.946	6.039
4×	0.469	0.577	0.115	2.309	2.383	4.897

Figure 11 presents the expanded uncertainties obtained for all calibration conditions and all independent gauge blocks.

The results indicate that the expanded uncertainty decreases systematically with increasing magnification. For all three gauge blocks, uncertainties at 1× and 2× magnifications are approximately 7 µm, whereas values at 4× magnification decrease to approximately 4.8–5.0 µm. This behaviour is directly related to the lower MPE specified by the microscope manufacturer for higher magnifications.

A comparison of the individual calibration conditions shows that the influence of calibration artefact geometry on the expanded uncertainty is relatively small. Although certain calibration conditions exhibit slightly higher uncertainty values, the differences between linear and circular artefacts remain substantially smaller than the uncertainty

contribution associated with the microscope MPE. Consequently, the selection of calibration artefact geometry does not represent the dominant source of uncertainty in the investigated measurement system.

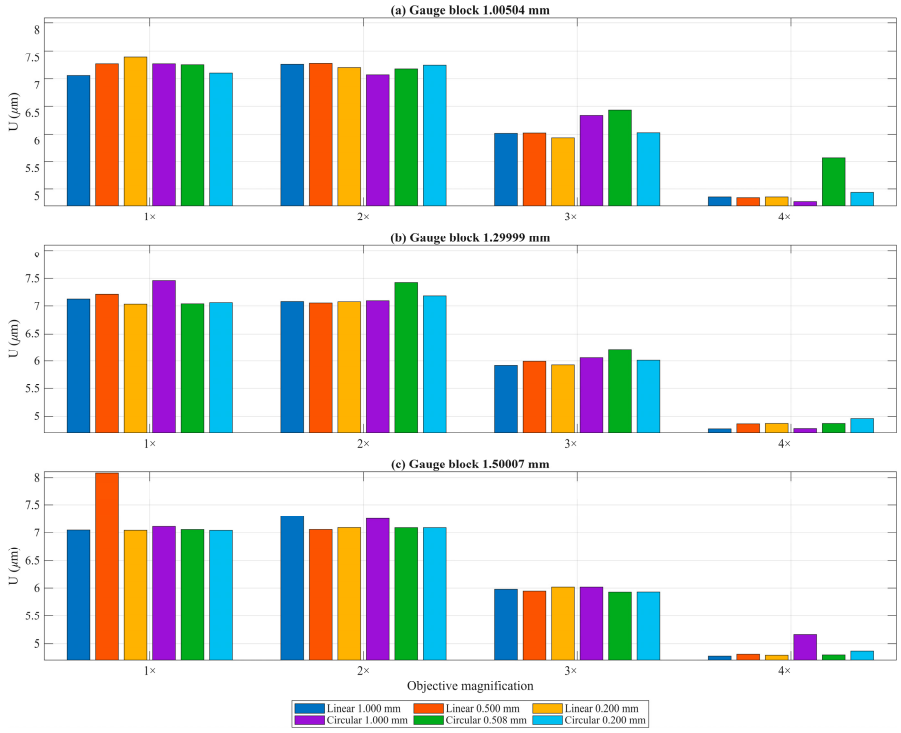


Figure 11. Expanded uncertainty obtained for independent ceramic gauge blocks after calibration using different linear and circular artefacts: (**a**) 1.00504 mm, (**b**) 1.29999 mm, and (**c**) 1.50007 mm. All subplots share the same vertical scale.

To better understand the relative importance of individual uncertainty sources, the average contribution of each component was analysed as shown in Figure 12.

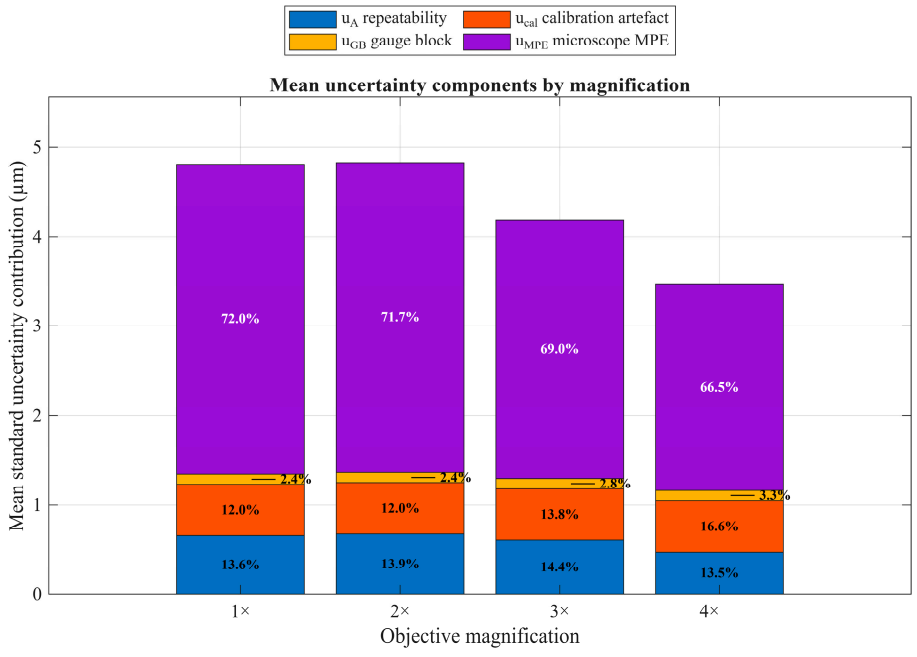


Figure 12. Relative contribution of uncertainty components as a function of objective magnification.

The contribution analysis reveals that the microscope MPE is the dominant uncertainty component for all investigated magnifications. At 1× and 2× magnifications, the MPE contribution accounts for approximately 72% of the total uncertainty budget. At 3× magnification, its contribution decreases slightly to approximately 69%, while at 4× magnification it remains the largest component with a contribution of approximately 66.5%.

The reduction in uncertainty with increasing magnification is primarily caused by the lower MPE values specified by the microscope manufacturer (Table 1), rather than by changes in the calibration artefact geometry.

The contribution of repeatability (u_A) varies between 13.5% and 14.4%, whereas the calibration artefact contribution (u_{cal}) ranges from 12.0% to 16.6%. The contribution of the reference gauge blocks (u_{GB}) remains the smallest component, accounting for only 2.4–3.3% of the total uncertainty budget.

These findings demonstrate that the overall measurement uncertainty is governed primarily by the intrinsic performance of the microscope rather than by the choice of calibration artefact geometry. Although statistically significant differences between calibration conditions were identified in Section 3.4, their practical metrological impact on the uncertainty budget is limited when compared with the dominant contribution of the microscope MPE. Therefore, improvements in measurement performance are more likely to be achieved through reductions in instrument MPE and repeatability errors than through modifications of calibration artefact geometry alone.

4. Discussion

The objective of this study was to investigate whether the geometry of a calibration artefact influences the metrological performance of a pixel-based optical measuring microscope. The experimental results demonstrated that both calibration artefact geometry and calibration dimension affect the resulting calibration coefficients and subsequent dimensional measurements. However, the magnitude of this influence depends strongly on the selected magnification and the size of the measured feature.

The analysis of calibration coefficients revealed measurable differences between the linear and circular calibration artefacts. The largest discrepancies were generally observed for the smallest calibration dimension (0.200 mm) and at lower magnifications, whereas the differences decreased substantially as magnification increased. At 4× magnification, several calibration conditions produced nearly identical calibration coefficients regardless of artefact geometry. This behaviour can be explained by the increased number of pixels representing a given physical feature at higher magnifications. As the image sampling density increases, the influence of pixel quantization, edge localization uncertainty, and image noise on the calibration coefficient becomes progressively smaller.

It should also be noted that the nominal dimensions of the available calibration targets were not completely identical. The linear calibration target employed a nominal dimension of 0.500 mm, whereas the corresponding circular target had a nominal dimension of 0.508 mm. Although the relative difference of approximately 1.6% is small, it represents a limitation of the present study because the comparison was performed using the commercially available calibration targets supplied with the microscope. Consequently, part of the observed differences may originate not only from calibration target geometry but also from the slight difference in nominal calibration dimension. This limitation should be considered when interpreting the quantitative comparison between these two calibration conditions.

Although the nominal dimensions of the corresponding linear and circular calibration targets differ by approximately 1.6%, the calibration coefficient is inherently determined as the ratio between the nominal calibration dimension and the measured pixel distance. Consequently, the calibration coefficient itself represents a normalized quantity rather than

an absolute dimensional measurement. Therefore, the observed differences cannot be attributed solely to the difference in nominal target dimensions. The relative difference between the nominal calibration dimensions (1.6%) is considerably smaller than the declared microscope MPE (±4–6 µm) and therefore is not expected to dominate the overall measurement uncertainty. Nevertheless, the slight dimensional mismatch remains a limitation of the present study and should be considered when interpreting quantitative comparisons between the two calibration target geometries.

The verification measurements performed using independent ceramic gauge blocks confirmed that the differences observed during calibration propagate into dimensional measurements. Nevertheless, the magnitude of the resulting deviations remained relatively small. Although statistically significant differences were identified for numerous calibration conditions, no universal superiority of either the linear or circular calibration artefact was observed. Depending on the magnification and measured gauge block, both calibration strategies produced either smaller or larger deviations. This finding indicates that the relationship between calibration artefact geometry and measurement performance is more complex than a simple comparison between linear and circular reference standards.

The statistical analysis demonstrated that calibration conditions can significantly influence measurement results. Nine of the twelve investigated combinations of gauge block dimension and magnification produced statistically significant Kruskal–Wallis test results. Furthermore, several experimental conditions exhibited medium or large effect sizes according to the epsilon-squared coefficient. These findings indicate that calibration strategy should not be regarded merely as a routine adjustment procedure but rather as a factor capable of affecting measurement performance. At the same time, statistical significance should not be interpreted as direct evidence of practical metrological importance. The uncertainty analysis showed that the dominant contribution to the overall uncertainty budget originated from the microscope maximum permissible error. Depending on magnification, the MPE contribution accounted for approximately 66–72% of the total uncertainty budget, whereas the contribution associated with the calibration artefacts represented only about 12–17%. The uncertainty contribution of the reference gauge blocks remained below 4% in all cases. Consequently, although calibration artefact geometry influences the measurement process, the overall measurement uncertainty is governed primarily by the intrinsic performance of the optical measuring system.

From a practical metrological perspective, this finding indicates that improvements in calibration target geometry alone are unlikely to produce substantial reductions in the overall measurement uncertainty of this microscope. Since the manufacturer's MPE represents approximately two-thirds of the total uncertainty budget, further improvements in measurement accuracy are expected to be achieved more effectively through improvements in the optical measuring system itself, such as enhanced optical quality, improved mechanical stability, higher image sensor resolution, or a reduction in the instrument MPE. Consequently, the selection of calibration target geometry should be regarded as an optimization of the calibration procedure rather than the primary factor determining the achievable measurement accuracy.

The uncertainty analysis presented in this study is intentionally conservative because the microscope MPE was taken directly from the manufacturer's specification. In practical applications, the effective measurement error for a specific measurement task may be considerably smaller than the declared MPE, particularly when measurements are performed over a limited measuring range, at fixed magnifications, and under controlled laboratory conditions. Consequently, laboratories requiring lower uncertainty may benefit from experimentally evaluating the actual measurement performance of the microscope for their specific application rather than relying solely on the manufacturer's specification.

Furthermore, a more comprehensive uncertainty budget could explicitly include additional influence quantities such as environmental stability, illumination uniformity, focus repeatability, field-of-view position, and image-processing repeatability. Although these effects were minimized during the present investigation by controlled laboratory conditions and standardized measurement procedures, their individual contributions were not evaluated separately. Such an extended uncertainty analysis represents an interesting direction for future work and may reduce the relative dominance of the manufacturer's MPE within the total uncertainty budget.

The observed dependence on magnification is particularly noteworthy. In the investigated microscope, the manufacturer-specified MPE decreases from ± 6 µm at $1\times$ and $2\times$ magnifications to ± 4 µm at $4\times$ magnification. Therefore, a portion of the observed improvement can be attributed directly to the enhanced metrological characteristics of the instrument at higher magnifications. Nevertheless, similar qualitative behaviour would likely be expected even in microscopes exhibiting a constant MPE across all magnifications. Increasing magnification generally increases the number of pixels representing the measured feature, thereby reducing discretization effects and improving feature localization independently of the declared MPE. The magnitude of the improvement would likely differ, but the overall trend would be expected to remain similar.

The smallest calibration dimension investigated in this study, namely 0.200 mm, consistently produced the largest differences between calibration conditions. A plausible explanation is that smaller calibration features occupy fewer pixels in the acquired image. Under such circumstances, the calibration coefficient becomes increasingly sensitive to edge detection algorithms, threshold selection, image noise, optical blur, and sub-pixel interpolation procedures. This interpretation is consistent with previous findings reported in machine vision metrology, where small image features are often associated with increased uncertainty and reduced repeatability. Conversely, larger calibration dimensions are represented by a greater number of pixels, reducing the influence of local edge detection errors. However, when dimensions become significantly larger, other effects such as lens distortion, stage positioning errors, and field non-uniformity may become increasingly important.

The present results were obtained for calibration dimensions ranging from 0.200 mm to 1.000 mm. Although these dimensions are representative of many practical calibration procedures used in optical microscopy, caution should be exercised when extrapolating the results to substantially smaller or larger dimensions. For dimensions below approximately 100 µm, the influence of calibration artefact geometry is expected to increase because the calibration coefficient would be determined from a very limited number of pixels. Under such conditions, sub-pixel edge localization and image-processing algorithms may become dominant contributors to measurement uncertainty. Conversely, for dimensions extending over several millimetres, the influence of local feature geometry may decrease, while optical distortion and field-dependent effects may become more significant.

Based on the investigated optical measuring microscope and the experimental conditions considered in this study, calibration dimensions in the range of approximately 0.5–1.0 mm provided stable calibration coefficients, satisfactory verification performance, and low measurement uncertainty. These dimensions may therefore serve as a practical guideline for similar image-based optical measurement systems. However, they should not be regarded as universally optimal. Since the optimum calibration dimension depends on the optical configuration, field of view, image sensor, magnification range, and measurement algorithm, each laboratory is encouraged to evaluate its own measurement system using the experimental methodology proposed in this work before establishing routine calibration procedures.

The optical design of the microscope should also be considered when interpreting the results. The investigated system represents a pixel-based optical measuring microscope in which dimensional measurements are derived from image coordinates. Several design characteristics may influence the sensitivity of such systems to calibration artefact geometry, including objective lens distortion, telecentricity, image sensor resolution, pixel size, illumination conditions, and image-processing algorithms. In particular, non-telecentric optical systems may exhibit increased sensitivity to object position and focus level, potentially amplifying differences between calibration artefacts. Similarly, image sensors with larger pixels or lower resolution may increase the influence of feature localization errors when small calibration dimensions are used. Consequently, although the qualitative trends identified in this study are expected to remain valid for similar image-based measuring systems, the quantitative values should not be interpreted as universally applicable to all microscope designs.

The investigated microscope employs a non-telecentric optical configuration. Consequently, dimensional measurements may be affected by small variations in object position, focus level, and feature location within the field of view. Telecentric optical systems would be expected to exhibit lower sensitivity to such effects. Therefore, the quantitative values reported in this study should be interpreted within the context of the investigated optical configuration.

Another aspect that deserves consideration is the spatial position of the measured feature within the field of view. The present investigation was performed using measurements acquired near the central region of the image, where optical distortion is typically minimized. In practical applications, however, distortion is often position-dependent and may vary significantly between the centre and the edges of the image. Therefore, calibration coefficients determined using features located near the image centre may not fully represent measurement performance across the entire field of view. Future investigations should evaluate calibration artefact geometry as a function of image position and generate two-dimensional calibration maps covering the complete measurement area. Such studies would provide valuable insight into the interaction between artefact geometry, optical distortion, and measurement uncertainty.

Several limitations of the present work should also be acknowledged. First, the investigation was performed using a single optical measuring microscope. Although the selected instrument represents a typical pixel-based measurement system, additional studies involving microscopes from different manufacturers, optical configurations, and accuracy classes would be beneficial for assessing the generality of the observed trends. Second, only one type of linear and one type of circular calibration artefact were considered. Additional studies involving grid standards, checkerboard artefacts, dot arrays, photomasks, and other machine vision calibration standards could provide a broader understanding of the relationship between calibration artefact geometry and measurement performance. Third, only ten repeated measurements were available for each experimental condition. While this number is sufficient for evaluating repeatability and performing non-parametric statistical analysis, larger datasets would enable a more comprehensive probabilistic characterization of measurement variability.

Although individual optical aberrations were not quantified in the present study, no visually significant image degradation such as severe distortion or defocus was observed during the calibration and verification measurements. Consequently, the observed differences between calibration conditions are considered to originate primarily from the calibration procedure itself rather than from evident optical defects of the imaging system.

Although the numerical results reported in this study are specific to the investigated optical measuring microscope and the corresponding experimental conditions, the proposed

experimental methodology is not limited to this particular instrument. The combination of calibration coefficient evaluation, independent verification using reference gauge blocks, statistical hypothesis testing, effect size analysis, and uncertainty evaluation constitutes a general framework for assessing the influence of calibration target geometry in image-based dimensional metrology. Consequently, the methodology can be readily applied to other optical measuring systems to evaluate their sensitivity to different calibration strategies.

Future research should therefore focus on expanding the range of investigated microscope designs, calibration artefacts, and calibration dimensions. Particular attention should be given to field-of-view mapping, distortion compensation, and the influence of sub-pixel feature extraction algorithms. The extension of the proposed methodology to telecentric optical systems, automated machine vision platforms, and three-dimensional optical measuring instruments such as focus variation and confocal microscopy systems also represents a promising direction for future investigation.

Overall, the results indicate that calibration artefact geometry influences calibration coefficients and dimensional measurement results, but its practical metrological impact depends strongly on magnification, calibration dimension, and instrument characteristics. While statistically significant differences may occur, the dominant factor governing measurement uncertainty remains the intrinsic performance of the optical measuring system. Consequently, calibration artefact geometry should be considered as one element of a broader measurement chain rather than as an isolated determinant of measurement accuracy.

5. Conclusions

In this study, the influence of calibration artefact geometry on the metrological performance of a pixel-based optical measuring microscope was systematically investigated. Linear and circular calibration artefacts with nominal dimensions of 1.000 mm, 0.500/0.508 mm, and 0.200 mm were used to determine calibration coefficients at four objective magnifications (1×–4×). The resulting calibration coefficients were subsequently validated using independent Grade 1 ceramic gauge blocks with nominal dimensions of 1.00504 mm, 1.29999 mm, and 1.50007 mm. Statistical analysis and uncertainty evaluation were performed to quantify the influence of calibration artefact geometry on dimensional measurement results.

The main contributions and findings of the study can be summarized as follows:

(a) Quantitative evaluation of calibration artefact geometry influence. The study demonstrated that calibration coefficients obtained from linear and circular artefacts are not identical and that the observed differences depend on both calibration dimension and magnification. The largest discrepancies were observed for the smallest calibration dimension (0.200 mm), whereas the differences generally decreased with increasing magnification. These results confirm that calibration artefact geometry affects the determination of the pixel-to-length conversion coefficient in image-based measuring systems.

(b) Experimental verification using independent reference standards. Unlike many calibration studies that evaluate only calibration coefficients, the proposed methodology included verification measurements using independent ceramic gauge blocks. This approach enabled the practical impact of calibration artefact selection on dimensional measurements to be quantified. Although measurable differences were observed between calibration conditions, all verification measurements remained within the declared maximum permissible error of the microscope.

(c) Comprehensive statistical assessment of calibration conditions. A statistical framework combining Kruskal–Wallis testing, Dunn–Šidák post hoc analysis and effect size evaluation was applied. The analysis revealed statistically significant differences in

nine of the twelve investigated combinations of gauge block dimension and magnification. The calculated effect sizes ranged from negligible to large, indicating that calibration conditions can significantly influence measurement results depending on the measurement scenario.

(d) Measurement uncertainty evaluation. The uncertainty analysis demonstrated that the dominant contribution to the uncertainty budget originated from the microscope maximum permissible error. Depending on magnification, the MPE contribution represented approximately 66–72% of the total uncertainty budget, whereas the contribution associated with calibration artefacts remained substantially smaller. Although calibration artefact geometry influenced the measurement results, its impact on the overall uncertainty budget was limited compared with the intrinsic performance characteristics of the measuring system.

(e) Practical implications for optical microscope calibration. For the investigated optical measuring microscope and the experimental conditions considered in this study, both investigated calibration target geometries provided satisfactory calibration performance and verification results within the declared metrological characteristics of the instrument. The numerical results reported in this study should therefore not be interpreted as universally applicable to all optical measuring microscopes but rather as representative of the investigated measurement system. The principal contribution of the present work is the proposed experimental methodology for comparing calibration target geometries, which can be readily applied to other optical measuring systems. However, calibration dimensions of approximately 0.5–1.0 mm exhibited more stable behaviour and lower sensitivity to artefact geometry than the smallest investigated calibration dimension (0.2 mm). Therefore, calibration dimensions within this range are recommended whenever practical measurement conditions allow.

The results further demonstrated that the influence of calibration artefact geometry cannot be considered independently of magnification, calibration dimension, image resolution, and microscope design. While statistically significant differences may occur between calibration strategies, the overall measurement uncertainty remains primarily governed by the metrological characteristics of the optical measuring system itself.

Several limitations of the present work should be acknowledged. The investigation was conducted using a single microscope operating on a pixel-based measurement principle, and only one linear and one circular calibration artefact were evaluated. Consequently, the quantitative results should not be interpreted as universally applicable to all optical measuring microscopes. Nevertheless, the proposed methodology is sufficiently general to be applied to other image-based measurement systems.

The calibration dimensions identified in this work should therefore be regarded as practical guidelines for the investigated measurement system rather than universally optimal values. The proposed methodology enables other laboratories to determine the most appropriate calibration conditions for their own optical measuring microscopes.

From a practical point of view, the proposed methodology enables laboratories to determine whether measurement performance is limited primarily by the calibration procedure or by the intrinsic characteristics of the measuring instrument. In the investigated microscope, the uncertainty budget was dominated by the manufacturer-specified MPE, indicating that further improvements in calibration target geometry alone are unlikely to produce substantial improvements in overall measurement accuracy. Therefore, before investing in alternative calibration targets, laboratories should first evaluate the relative contributions of individual uncertainty components. If the instrument MPE dominates the uncertainty budget, improving the calibration artefact alone may have only a limited influence on the final measurement performance.

Future research should focus on extending the proposed methodology to microscopes with different optical configurations, telecentric and non-telecentric optical systems, alternative calibration artefact geometries, and larger calibration ranges. Additional investigations should also examine field-of-view dependence, distortion compensation, sub-pixel feature extraction algorithms, and calibration procedures for advanced optical measuring systems such as focus variation and confocal microscopes.

Future work will focus on experimentally determining application-specific uncertainty contributions and replacing conservative specification-based uncertainty components with experimentally validated estimates wherever appropriate.

In conclusion, the principal contribution of this work is not the specific numerical values obtained for the investigated microscope, but the development and validation of a comprehensive experimental methodology for evaluating the influence of calibration target geometry on pixel-based dimensional measurements. The proposed methodology combines calibration coefficient analysis, independent verification, statistical evaluation, and uncertainty analysis and can therefore be applied to other image-based optical measuring systems to support objective comparison of alternative calibration strategies.

Author Contributions: Conceptualization, D.M.; Software, D.M.; Validation, D.M.; Formal analysis, D.M.; Investigation, D.M., T.K. and M.K.; Resources, T.K.; Data curation, T.K.; Writing—review and editing, M.K.; Supervision, T.K. and M.K.; Project administration, M.K. All authors have read and agreed to the published version of the manuscript.

Funding: The authors would like to thank the Slovak Grant Agency—project VEGA 1/0191/24, and project KEGA 004TUKE-4/2024.

Institutional Review Board Statement: Not applicable.

Informed Consent Statement: Not applicable.

Data Availability Statement: The original contributions presented in this study are included in the article. Further inquiries can be directed to the corresponding author.

Conflicts of Interest: The authors declare no conflicts of interest.

References

1. Bergmann, R.B.; Kalms, M.; Falldorf, C. Optical In-Process Measurement: Concepts for Precise, Fast and Robust Optical Metrology for Complex Measurement Situations. *Appl. Sci.* **2021**, *11*, 10533. [CrossRef]
2. Dai, G.; Neugebauer, M.; Stein, M.; Bütefisch, S.; Neuschaefer-Rube, U. Overview of 3D Micro- and Nanocoordinate Metrology at PTB. *Appl. Sci.* **2016**, *6*, 257. [CrossRef]
3. Schwenke, H.; Neuschaefer-Rube, U.; Pfeifer, T.; Kunzmann, H. Optical methods for dimensional metrology in production engineering. *CIRP Ann.* **2002**, *51*, 685–699. [CrossRef]
4. Harding, K. *Handbook of Optical Dimensional Metrology*; CRC Press: Boca Raton, FL, USA, 2013. [CrossRef]
5. Leach, R. *Optical Measurement of Surface Topography*; Springer: Berlin/Heidelberg, Germany, 2011. [CrossRef]
6. Gao, W.; Haitjema, H.; Fang, F.Z.; Leach, R.K.; Cheung, C.F.; Savio, E.; Linares, J.M. On-machine and in-process surface metrology for precision manufacturing. *CIRP Ann.* **2019**, *68*, 843–866. [CrossRef]
7. Zhang, Z. A flexible new technique for camera calibration. *IEEE Trans. Pattern Anal. Mach. Intell.* **2000**, *22*, 1330–1334. [CrossRef]
8. Luhmann, T.; Robson, S.; Kyle, S.; Boehm, J. *Close-Range Photogrammetry and 3D Imaging*; Walter de Gruyter: Berlin, Germany, 2013. [CrossRef]
9. Khan, M.F.; Dannoun, E.M.A.; Nofal, M.M.; Mursaleen, M. Significance of Camera Pixel Error in the Calibration Process of a Robotic Vision System. *Appl. Sci.* **2022**, *12*, 6406. [CrossRef]
10. Ge, R.; Li, D.; Zhang, X.; Wang, R.; Zheng, W.; Li, X.; Zhao, W. Comparison of Camera Calibration and Measurement Accuracy Techniques for Phase Measuring Deflectometry. *Appl. Sci.* **2021**, *11*, 10300. [CrossRef]
11. Zhu, Y.; Cheng, Y.; Gao, H.; Sun, S.; Zhang, X.; Xue, L.; Tang, J.; Tang, Y. High-Precision Measurement of Microscales Based on Optoelectronics and Image Integration Method. *Micromachines* **2024**, *15*, 1162. [CrossRef] [PubMed]
12. Yuan, K.; Fu, H.; Li, R.; Shen, L.; Qian, L.; Qin, D.; Wu, H. Research on sub-pixel detection and evaluation of round-ness error of shaft workpiece based on machine vision. *J. Mech. Sci. Technol.* **2025**, *39*, 2041–2049. [CrossRef]

13. *JCGM 100:2008*; Evaluation of Measurement Data—Guide to the Expression of Uncertainty in Measurement. JCGM: Sèvres, France, 2008.
14. Hemming, B. Measurement Traceability and Uncertainty in Machine Vision Applications. Doctoral Dissertation, Aalto Uniersity, Espoo, Finland, 2007.
15. Coveney, T. *The Measurement of Features Using Vision Systems*; Good Practice Guide No. 39; National Physical Laboratory: Teddington, UK, 2014.
16. *ISO 10360-7:2011*; Geometrical Product Specifications (GPS)—Acceptance and Reverification Tests for Coordinate Measuring Machines Equipped with Imaging Probing Systems. ISO: Geneva, Switzerland, 2011.
17. Li, Q.; Shimizu, Y.; Saito, T.; Matsukuma, H.; Gao, W. Measurement Uncertainty Analysis of a Stitching Linear-Scan Method for the Evaluation of Roundness of Small Cylinders. *Appl. Sci.* **2020**, *10*, 4750. [CrossRef]
18. Cheng, Y.; Wang, Z.; Chen, X.; Li, Y.; Li, H.; Li, H.; Wang, H. Evaluation and Optimization of Task-oriented Measurement Uncertainty for Coordinate Measuring Machines Based on Geometrical Product Specifications. *Appl. Sci.* **2019**, *9*, 6. [CrossRef]
19. Leach, R. *Fundamental Principles of Engineering Nanometrology*; Elsevier: Amsterdam, The Netherlands, 2014.
20. De Groot, P.J. The Meaning and Measure of Vertical Resolution in Optical Surface Topography Measurement. *Appl. Sci.* **2017**, *7*, 54. [CrossRef]
21. Hua, T.; Xie, H.; Wang, S.; Hu, Z.; Chen, P.; Zhang, Q. Evaluation of the quality of a speckle pattern in the digital image correlation method by mean subset fluctuation. *Opt. Laser Technol.* **2010**, *43*, 9–13. [CrossRef]
22. Sáenz-Nuño, M.A.; Marín, M.M.; Puente, C.; Rubio, E.M. Zone-Based Interim Verification Method for 2D Vision Measurement Systems Using Non-Calibrated Artifacts: Performance, Spatial Consistency, and Future Applications. *Appl. Sci.* **2026**, *16*, 3032. [CrossRef]
23. Zaremba, A.; Nitkiewicz, S. Distance Estimation with a Stereo Camera and Accuracy Determination. *Appl. Sci.* **2024**, *14*, 11444. [CrossRef]
24. Carmignato, S.; De Chiffre, L.; Bosse, H.; Leach, R.K.; Balsamo, A.; Estler, W.T. Dimensional artefacts to achieve metrological traceability in advanced manufacturing. *CIRP Ann.* **2020**, *69*, 693–716. [CrossRef]
25. Doiron, T.D. Grid plate calibration at the National Bureau of Standards. *J. Res. Natl. Bur. Stand.* **1988**, *93*, 41. [CrossRef]
26. Shilling, M.; Tran, H.D.; Claudet, A.A.; Oliver, A.D.; Bauer, T.M. Silicon Bulk Micromachined Hybrid Dimensional Artifact. *NCSLI Meas.* **2010**, *5*, 56–65. [CrossRef]
27. Meli, F. *Calibration of Photomasks for Optical Coordinate Metrology*; Physikalisch-Technische Bundesanstalt (PTB): Braunschweig, Germany, 2013. Available online: https://oar.ptb.de/resources/show/10.7795/810.20130620C (accessed on 21 July 2026).
28. National Institute of Standards and Technology (NIST). Nanostructure Dimension Calibration. Available online: https://www.nist.gov/pml/applied-physics-division/products-services/nanostructure-dimension-calibration (accessed on 21 July 2026).
29. Swyt, D.A. Length and Dimensional Measurements at NIST. *J. Res. Natl. Inst. Stand. Technol.* **2001**, *106*, 1–23. [CrossRef] [PubMed]
30. *VDI/VDE 2634*; Optical 3D Measuring Systems—Acceptance and Reverification Tests. Beuth Verlag GmbH: Berlin, Germany, 2012.
31. Costa, P.B.; Marques, A.; Baldner, F.O.; Leta, F.R. Line scale measurement using image registration. *Int. J. Metrol. Qual. Eng.* **2013**, *4*, 121–125. [CrossRef]
32. Muñoz-Gómez, J.A.; Galvan, C. Robust line detection for line scale calibration. In *Series on Advances in Mathematics for Applied Sciences*; World Scientific: Singapore, 2009; pp. 243–248. [CrossRef]
33. National Physical Laboratory (NPL). Precision Scales, Stage Micrometers and Graticules for Optical Calibration. Available online: https://www.npl.co.uk/products-services/dimensional/scales-micrometers (accessed on 21 July 2026).
34. Peng, T.; Gu, A.; Fang, D.; Zhang, Z. High-precision camera calibration based on concentric circle compensation for industrial environments. *Opt. Express* **2025**, *33*, 52503. [CrossRef] [PubMed]
35. Ghazouali, S.E.; Vissiere, A.; Lafon, L.-F.; Bouazizi, M.-L.; Nouira, H. Optimised calibration of machine vision system for close range photogrammetry based on machine learning. *J. King Saud Univ. Comput. Inf. Sci.* **2022**, *34*, 7406–7418. [CrossRef]
36. Wang, X.; Yao, T.; Shi, Z. Calibration Method Based on Virtual Gear Artefact for Computer Vision Measuring Instrument of Fine Pitch Gear. *Sensors* **2024**, *24*, 2289. [CrossRef] [PubMed]
37. Gadelmawla, E.; Khalifa, W.; Elewa, I. Measurement and Inspection of Roundness Using Computer Vision (Dept.M). *MEJ Mansoura Eng. J.* **2020**, *33*, 20–32. [CrossRef]
38. Vorburger, T.; Blateyron, F. *Surface Metrology and Optical Measurement Methods*; Springer: Berlin/Heidelberg, Germany, 2011.
39. Vanrusselt, M.; Haitjema, H. Characterization of measurement and instrument noise in areal surface topography measurements by the Allan deviation. *CIRP Ann.* **2023**, *72*, 485–488. [CrossRef]
40. Poon, C.Y.; Bhushan, B. Comparison of surface roughness measurements by stylus profiler, AFM and non-contact optical profiler. *Wear* **1995**, *190*, 76–88. [CrossRef]
41. Chen, L.-C.; Duong, D.-H.; Chen, C.-S. Optical 3-D Profilometry for Measuring Semiconductor Wafer Surfaces with Extremely Variant Reflectivities. *Appl. Sci.* **2019**, *9*, 2060. [CrossRef]

42. Gao, S.; Felgner, A.; Brand, U. Metrological-Characteristics-Based Calibration of Optical Areal Surface Measuring Instruments and Evaluation of Measurement Uncertainty for Surface Texture Measurements. *Instruments* **2025**, *9*, 11. [CrossRef]
43. Ito, S.; Kikuchi, H.; Chen, Y.; Shimizu, Y.; Gao, W.; Takahashi, K.; Kanayama, T.; Arakawa, K.; Hayashi, A. A Micro-Coordinate Measurement Machine (CMM) for Large-Scale Dimensional Measurement of Micro-Slits. *Appl. Sci.* **2016**, *6*, 156. [CrossRef]
44. Villarraga-Gómez, H.; Lee, C.; Smith, S.T. Dimensional metrology with X-ray CT: A comparison with CMM measurements on internal features and compliant structures. *Precis. Eng.* **2017**, *51*, 291–307. [CrossRef]
45. Savio, E.; De Chiffre, L.; Schmitt, R. Metrology of freeform shaped parts. *CIRP Ann.* **2007**, *56*, 810–835. [CrossRef]
46. Weckenmann, A.; Knauer, M.; Kunzmann, H. The influence of measurement strategy on the uncertainty of CMM-Measurements. *CIRP Ann.* **1998**, *47*, 451–454. [CrossRef]
47. De Chiffre, L.; Carmignato, S.; Kruth, J.-P.; Schmitt, R.; Weckenmann, A. Industrial applications of computed tomography. *CIRP Ann.* **2014**, *63*, 655–677. [CrossRef]
48. Remondino, F.; Fraser, C. Digital camera calibration methods: Considerations and comparisons. *Repos. Publ. Res. Data* **2006**, *36*, 266–272. [CrossRef]
49. Gąska, A.; Harmatys, W.; Gąska, P.; Kowaluk, T.; Styk, A.; Jakubowicz, M.; Swojak, N.; Stępień, K.; Wójtowicz, A. Hybrid Measuring System for Dimensional Metrology Tasks on Large-Volume Workpieces and Assessment of Its Uncertainty. *Appl. Sci.* **2026**, *16*, 1449. [CrossRef]
50. Craig, W.D.; Leeuwen, F.B.; Jarrett, S.R.; Hansen, R.S.; Berke, R.B. Using text as a native speckle pattern in digital image correlation. *J. Strain Anal. Eng. Des.* **2022**, *57*, 539–555. [CrossRef]
51. Peng, T.; Zhang, Z.; Chen, F.; Zeng, D. Dimension Measurement and Key Point Detection of Boxes through Laser-Triangulation and Deep Learning-Based Techniques. *Appl. Sci.* **2020**, *10*, 26. [CrossRef]
52. Saif, Y.; Rus, A.Z.M.; Yusof, Y.; Ahmed, M.L.; Al-Alimi, S.; Didane, D.H.; Adam, A.; Gu, Y.H.; Al-masni, M.A.; Abdulrab, H.Q.A. Advancements in Roundness Measurement Parts for Industrial Automation Using Internet of Things Architecture-Based Computer Vision and Image Processing Techniques. *Appl. Sci.* **2023**, *13*, 11419. [CrossRef]
53. Zhou, X.; Zhou, C.; Zhang, T.; Mou, X.; Xu, J.; He, Y. High Precision Visual Dimension Measurement Method with Large Range Based on Multi-Prism and M-Array Coding. *Sensors* **2022**, *22*, 2081. [CrossRef] [PubMed]
54. Bao, J.-P.; Wang, H.-S.; Zhang, X.-F. Calibration method of microscope and its measurement uncertainty. *Proc. SPIE Int. Soc. Opt. Eng. Proc. SPIE* **2006**, *6280*, 62802Y. [CrossRef]
55. Batista, E.; Furtado, A.; Ferreira, M.d.C.; Godinho, I.; Álvares, M.; Afonso, J.; Martins, R.F. Uncertainty Calculations in Optical Methods Used for Micro Flow Measurement. *Meas. Sens.* **2021**, *18*, 100155. [CrossRef]
56. Baumgartl, J.; Bechinger, C. On the limits of digital video microscopy. *Europhys. Lett.* **2005**, *71*, 487–493. [CrossRef]
57. Pawlus, P.; Reizer, R.; Wieczorowski, M.; Krolczyk, G.M. Sensitivities of surface texture parameters to measurement errors—A review. *Measurement* **2024**, *227*, 114323. [CrossRef]
58. Angermann, C.; Haltmeier, M.; Laubichler, C.; Jónsson, S.; Schwab, M.; Moravová, A.; Kiesling, C.; Kober, M.; Fimml, W. Surface topography characterization using a simple optical device and artificial neural networks. *Eng. Appl. Artif. Intell.* **2023**, *123*, 106337. [CrossRef]
59. *ISO 25178*; Geometrical Product Specifications (GPS)—Surface Texture: Areal. ISO: Geneva, Switzerland, 2021.
60. *ISO 21920*; Geometrical Product Specifications (GPS)—Surface Texture: Profile. ISO: Geneva, Switzerland, 2021.
61. *ISO 3650:2025*; Geometrical Product Specifications (GPS)—Length Standards—Gauge Blocks. International Organization for Standardization (ISO): Geneva, Switzerland, 2025.

Disclaimer/Publisher's Note: The statements, opinions and data contained in all publications are solely those of the individual author(s) and contributor(s) and not of MDPI and/or the editor(s). MDPI and/or the editor(s) disclaim responsibility for any injury to people or property resulting from any ideas, methods, instructions or products referred to in the content.